# Evidence for electron capture to the continuum by protons scattered at non-0° angles from Ar atoms

L. Sarkadi,[1] U. Brinkmann,[2] A. Báder,[1] R. Hippler,[2,*] K. Tökési,[1] and L. Gulyás[1]
[1]*Institute of Nuclear Research of the Hungarian Academy of Sciences (ATOMKI), P.O. Box 51, H-4001 Debrecen, Hungary*
[2]*Fakultät für Physik, Universität Bielefeld, D-33501 Bielefeld, Germany*
(Received 15 December 1997)

The process of electron capture to the continuum (ECC) has been studied at non-0° electron emission angles in a type of experiment in which the electrons ejected in a given direction are detected in coincidence with the outgoing projectiles scattered on the target nucleus in the same direction. Triply differential cross sections (differential with respect to the energy and angle of the ejected electron and the angle of the scattered projectile) have been determined for 75-keV proton on Ar collisions at scattering angles 3.7°, 5.0°, and 8.1°. The occurrence of the cusp peak in the coincidence spectra gives an evidence for the existence of the ECC process at non-0° emission angles. The experimental data are compared with results of first-order distorted-wave Born and classical trajectory Monte Carlo (CTMC) calculations. [S1050-2947(98)00307-2]

PACS number(s): 34.50.Fa

## I. INTRODUCTION

The most striking feature of the energy spectrum of the electrons ejected from ion-atom collisions in forward direction is a cusp-shaped peak appearing at the energy where the velocity of the electron matches that of the projectile, $v_e = v_p$. In case of target ionization the process leading to cusp is called *electron capture to the continuum* (ECC), because it can be visualized as a continuation of the bound-state capture across the continuum threshold. This collision phenomenon is known to be strongly affected by three-body effects. Although the ECC cusp was discovered a long time ago [1], it still represents a challenge for the theory, mainly because of the difficulties arising for the three-body system in the case of the long-range Coulomb force [2].

Most experiments for the cusp-electron production have been made measuring the electron spectrum at forward direction without further differentiation of the final state. The results of these experiments are generally well described by the different continuum-distorted-wave and impulse theories (for a review see, e.g., Refs. [3–5] and and references therein). A more thorough test of the theories can be achieved specifying the final state of the collision in a coincidence experiment. As examples, here we may mention the experiment [6] in which the contribution of the $L$ shell to the total cusp-electron production was determined in Ar, and two other experiments [7,8] in which the impact-parameter dependence of the process was investigated.

In the present work we obtained further differential information concerning the dynamics of ECC. It is known that the ECC cusp is characterized by a very strong angular dependence. The peak, which is intense and sharp at $\vartheta_e = 0°$, steeply decreases and broadens with increasing angle, and at $\vartheta_e = 10°$ practically disappears. The basic idea of this experiment is that a sharp electron cusp is expected to appear also at a ''non-0°'' emission angle, if the electron ejection is accompanied by a large-angle scattering of the projectile on the target nucleus in the same direction. For study of such a process one has to detect the electrons ejected in a given direction in coincidence with the projectiles emerging in the same direction.

The idea of the experiment is based on the assumption that the electron cusp is a result of final-state interaction between the ejected electron and the outgoing projectile [9,10]. This interpretation of the cusp is widely accepted. The corresponding theoretical calculations reproduce the properties of the electron cusp reasonably well. However, purely theoretically, one cannot exclude the existence of other mechanisms leading to cusp. One may assume, for example, that in the incoming phase of the collision the long-range Coulomb field of the projectile leads to such a distortion of the wave function that favors the electron ejection in the forward direction (''precollision'' interaction). The aim of the present work was to distinguish experimentally between the contributions of the precollision and postcollision interaction to the cusp production. The postcollision interaction is *directly* manifested in the above discussed experiment, i.e., observing the cusp at non-0° emission angles in coincidence with the projectiles scattered in the same direction. However, this experiment alone does not exclude the precollision cusp. Since the precollision interaction is expected to lead to electron ejection in the forward direction, its contribution to the cusp formation can be checked in another kind of experiment in which again collisions with large-angle scattering of the projectile are considered, but now the electrons are observed at $\vartheta_e = 0°$. The absence of a peak in the coincidence spectrum at $v_e = v_p$ excludes the cusp-electron production in the incoming phase of the collision.

Another importance of the present coincidence experiments is that selecting large-angle scatterings one can explore the collision region belonging to small impact parameters, and the obtained *triply* differential cross section data provide a base for a sensitive test of the different collision theories.

*Present address: Institut für Physik, Ernst-Moritz-Arndt Universität Greifswald, Domstrasse 10a, D-17487 Greifswald, Germany.

 

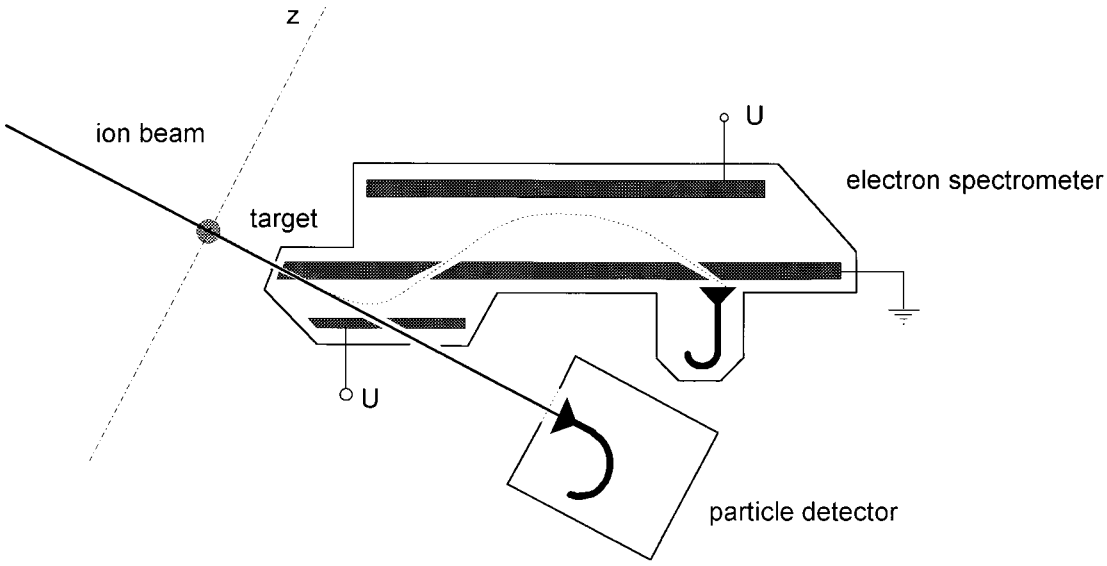


FIG. 1. Scheme of the experimental setup.

To demonstrate the above ideas, we carried out experiments for collisions of 75 keV protons with Ar atoms. The use of a heavy target atom and relatively small collision energy is justified by the requirement of the large cross section for large-angle scattering of the projectile. We used proton as a bombarding particle, mainly because the proton is the simplest bare projectile causing the smallest perturbation, and therefore the obtained data can be compared with the predictions of a perturbation theory. The proton projectile has also the advantage that the capture channel (simultaneous capture of two electrons: one into a bound state, another into a continuum state) is small in this case [11,12]. Although the cross section for both the ECC cusp production and the Rutherford scattering increases with decreasing impact energy, we could not use energy smaller than 75 keV for the following reasons. Firstly, we wanted to remain in the range of the validity of the first-order (distorted wave Born) ionization theory used for interpretation of the obtained data; secondly, at low impact energies one is faced with the difficulties of analyzing low-energy electrons (the electron detection efficiency sharply decreases below 30 eV).

## II. EXPERIMENTAL SETUP AND METHOD

The experiment was made at the 350 kV heavy-ion accelerator of the University of Bielefeld. The scheme of the experimental setup is shown in Fig. 1. A 75 keV collimated proton beam (1 mm diameter) crossed a thin Ar jet target. The ejected electrons were energy analyzed by a 30° double-stage parallel-plate electron spectrometer and counted by a channel electron multiplier (CEM). The spectrometer was characterized by an energy resolution of 3.2%. Its acceptance half-angles were $+4.6°$, $-6.4°$ in the focusing plane, and $\pm 1.8°$ in the plane perpendicular to the focusing plane. Behind the spectrometer the scattered protons were detected by a particle detector consisting of a CEM with integrated electronics (MD–501 Amptektron). The particle detector was fixed to the electron spectrometer. Its acceptance half-angle was $\pm 2.9°$. The electron spectrometer together with the particle detector was mounted on a turntable that could be rotated around the target with an angular uncertainty of 0.1°. The plane of the rotation in Fig. 1 is defined by the rotation axis $z$. To allow that the direct proton beam passes through the spectrometer, slits were cut into the entrance opening of the spectrometer and into the deflector plate of its first stage (perpendicularly to the plane of Fig. 1). This made it possible to rotate the spectrometer in the angular range of 0°–10°. The current of the direct proton beam was measured by a Faraday cup.

Special care was taken to suppress the background counts at the CEM of the particle detector due to the large number of electrons and recoiled target ions created by the proton beam with intensities of typically 0.1 nA. At the MD–501 Amptektron detector there is a possibility to bias the funnel of the CEM to $-400$ V in case of detection of positive ions. This possibility was used to repel the electrons. To get rid of the recoiled ions, we applied a high-transparency (90%) grid in front of the CEM biased to $+50$ V. Most of the experimental data had already been taken using this configuration, when it turned out that the detection efficiency for the scattered protons was very small, only about 10%. Furthermore, the profile of the detection efficiency as a function of the distance from the detector center had the shape of a Gaussian function, rather than a trapezoid function. The bad performance of the particle detector could be explained by the fact that the positively biased grid collected a significant part of the secondary electrons ejected by the protons from the funnel. To compensate for this effect, we put a negatively ($-400$ V) biased second grid between the first grid and the CEM. An increase of the counting efficiency by a factor of 3 was achieved in this way. Furthermore, after this modification the efficiency was constant on almost the entire input area of the detector.

Another source of the background counts of the particle detector was due to the protons scattered on the edge of the last beam collimator aperture and on the gas atoms between the collimator and the collision center. To prevent these protons from entering into the detector, a further collimator aperture with a hole of 2 mm diameter (not shown in Fig. 1)

was mounted just in front of the gas target.

Standard electronics were used to establish coincidences between the electrons and the scattered protons. The rate of the coincidence events was $N_c = 0.004-0.1\ \mathrm{s}^{-1}$, while the rates of the single events of the electrons and scattered protons were $N_e = 200-900\ \mathrm{s}^{-1}$ and $N_p = 400-3000\ \mathrm{s}^{-1}$, respectively. The validity of the condition of the single collision was checked measuring the yields of the single and coincidence events as a function of the target gas pressure. A linearity was found in a range where the pressure changed by a factor of 4.

From the yield of the single $N_e$ and coincidence $N_c$ electron events we have determined doubly and triply differential cross sections (DDCS's and TDCS's) in the following way. First let us consider DDCS's. $N_e$ can be expressed as

$$N_e = f_e \frac{d^2\sigma}{dE_e d\Omega_e} \Delta E_e\ \Delta\Omega_e\ \rho_t\ \Delta l\ n_p, \tag{1}$$

where $f_e$ is the electron detection efficiency (including the transmission of the spectrometer), $d^2\sigma/dE_e d\Omega_e$ is the DDCS for the electron ejection, $\Delta E_e$ and $\Delta\Omega_e$ are the energy window and the solid angle of the spectrometer, respectively, $\rho_t$ is the density of the target gas, $\Delta l$ is an effective target length, and $n_p$ is the number of the incoming protons. We did not measure absolute cross sections, but we determined relative DDCS values using the data of Rudd, Toburen, and Stolterfoht [13]. As reference cross sections we chose the DDCS data for 70 keV protons on Ar, at electron emission angle $\vartheta_e = 10°$. Using these data we determined the change of DDCS's when the proton energy was changed from 70 keV to 75 keV. This could be done at fixed angle, 10°. Since the angular range of our investigations was below 10° (where no reference cross sections exist), we had to calibrate the spectrometer also as a function of the angle. This was important because at small angles the ''extended target'' gives rise to an additional anisotropy in the observed electron emission. To make the angular calibration, we measured the intensity of the $M_{4,5}-NN$ Auger-line group of Kr centered at 53 eV at angles 0°, 3.7°, 5.0°, and 8.1°. The Auger electrons were excited by 200 keV protons. We have found that the Auger-electron yield was constant except for 0°, where it was higher by 13% than the average intensity at the other angles. Assuming isotropic angular distribution for the Auger-electron emission, we attributed the enhancement at 0° to the extended target effect, and it was taken into correction when the new DDCS values were determined. In this procedure we supposed that the dependence of $f_e$ on $\vartheta_e$ was negligible in the energy range of the measurements, i.e., effects other than the geometry of the target did not alter the angular distribution of the electrons.

The rate of the coincidence events can be expressed with TDCS as

$$N_c = f_e f_p \frac{d^3\sigma}{dE_e d\Omega_e d\Omega_p} \Delta E_e\ \Delta\Omega_e\ \Delta\Omega_p\ \rho_t\ \Delta l\ n_p, \tag{2}$$

where $f_p$ is the detection efficiency for the protons, $d^3\sigma/dE_e d\Omega_e d\Omega_p$ is the TDCS for the electron ejection, and $\Delta\Omega_p$ is the solid angle of the particle detector. Combining Eqs. (1) and (2), we find for TDCS

$$\frac{d^3\sigma}{dE_e d\Omega_e d\Omega_p} = \frac{1}{f_p \Delta\Omega_p} \frac{N_c}{N_e} \frac{d^2\sigma}{dE_e d\Omega_e}. \tag{3}$$

In this expression $N_c/N_e$ was directly obtained from the coincidence measurement, and the DDCS $d^2\sigma/dE_e d\Omega_e$ was determined as discussed above. $f_p\Delta\Omega_p$ was determined in a separate experiment in the following way. The electron spectrometer together with the particle detector was rotated to 0°, i.e., $\vartheta_e = \vartheta_p = 0°$. The intensity of the proton beam was lowered to a value small enough ($\propto 10^5$ protons/s) that the protons could be individually counted by the detector. We set the spectrometer voltage to the cusp maximum, and detected coincidences between the electrons and the protons. The ratio of the number of the coincidences to that of the single electron events gave directly the efficiency of the particle detector $f_p$. To this we assumed that for each detected electron the corresponding proton entered into the particle detector. This is a good assumption, since in relatively high-energy collisions the ionization take place at large internuclear distances (''distance collisions''), therefore the protons scatter in very small angles. Furthermore, for the ECC cusp the ejection of the electrons is characterized by an enhanced longitudinal momentum transfer corresponding to a narrow angular profile of the scattered projectiles [14]. In this manner, however, the detection efficiency was determined only in the *center* of the detector, $\vartheta_p = 0°$. To determine the product $f_p\Delta\Omega_p$, we had to check the uniformity of the detection efficiency over the entire input area of the detector. To do this, we removed the electron spectrometer from the turntable. Keeping the intensity of the proton beam at a constant value, we rotated the particle detector around 0° within its acceptance angle, and measured the proton count rate in angular steps of 0.3°. The obtained intensity distribution was normalized to the efficiency value measured at $\vartheta_p = 0°$. Since the efficiency profile was not uniform, we determined an *average* value for $f_p\Delta\Omega_p$, integrating the $f_p(\vartheta_p)$ function over the solid angle of the detector. For the case, when we had one grid in front of CEM, the integration yielded $\int f_p(\vartheta_p) d\Omega_p = 4.4\times 10^{-4}$.

## III. RESULTS AND DISCUSSION

As it was discussed in the Introduction, we carried out two kinds of coincidence experiments that differed in the relative positions of the electron spectrometer and the particle detector (see Fig. 2). In the arrangement shown by Fig. 2(a) the electrons observed at a given angle were detected in coincidence with the protons scattered in the same direction, i.e., $\vartheta_e = \vartheta_p$. The measurements in this geometry were made at angles 3.7°, 5.0°, and 8.1°. The obtained DDCS and TDCS values have been plotted in Fig. 3. The figure includes also the DDCS data obtained for the cusp at $\vartheta_e = 0°$ in a separate noncoincidence experiment. The errors shown for the TDCS data are mainly statistical errors, but they also contain a reproducibility error that was estimated to be 10%. The latter was caused by the change of the detection efficiency during the long-time coincidence measurements. For DDCS the statistical errors were negligibly small. In addition to the above errors, a systematic error of about 25% resulting from normalization to the absolute cross section data of Rudd, Toburen, and Stolterfoht [13] contributes to the total uncertainty

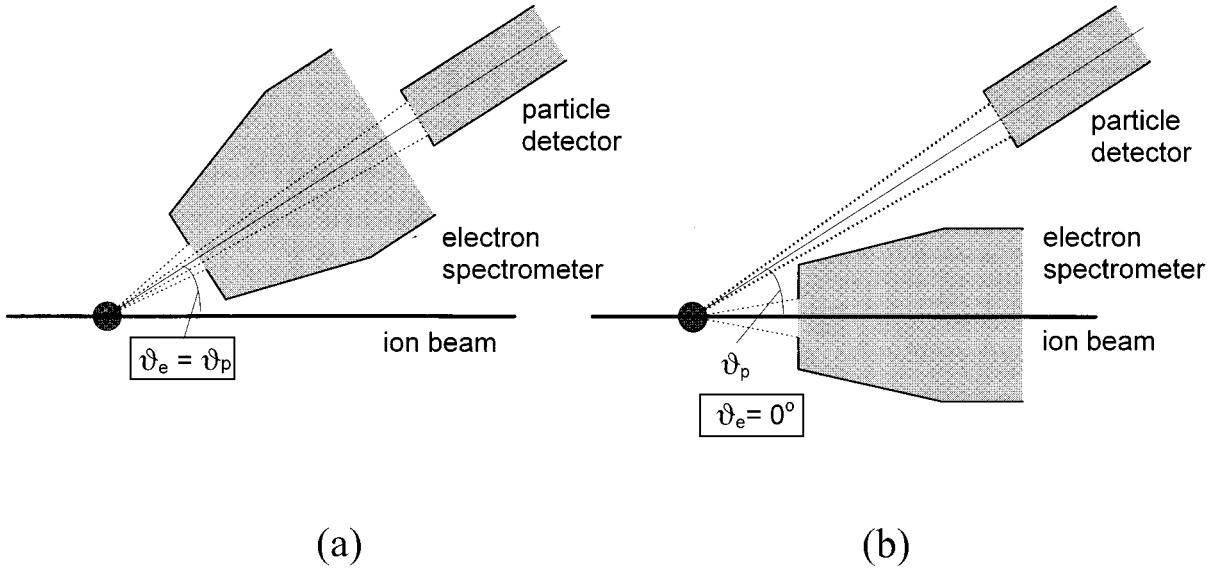


FIG. 2. Detection geometries for the electrons and the scattered ions. (a) Identical observation angles; (b) different observation angles.

of the measured cross sections.

From Fig. 3(a) one can see the rapid change of the shape of DDCS with increasing angle. The cusp that dominates the spectrum at 0° practically disappears at 8.1°. At the same time, the electron spectra obtained in coincidence with the scattered protons [Fig. 3(b)] have similar cusp shapes at each of the observation angles, proving the existence of the ECC process at non-zero-degree emission angles.

The shape of the cusp observed in coincidence with the scattered protons seems to be different from that observed at 0° in the noncoincidence experiment. Of course, one does not expect completely identical shapes, since the spectra observed at larger angles belong to collisions with small impact parameters, while the spectrum at 0° comes from distance collisions, i.e., the dynamics for the cusp production is different for the two cases. Apart from such ''physical'' difference, one has to regard that for coincident detection the sharp cusp shape is partly smeared out by the finite angular resolution of the particle detector. This means that to obtain a spectrum that can be directly compared with the coincidence spectra, the spectrum at 0° has to be *convoluted* with the response function of the particle detector.

To take into account the smearing effect, in a separate (noncoincidence) measurement we took electron spectra around 0° in angular steps of 0.65° within the acceptance angle of the particle detector, and integrated these spectra over the solid angle of the detector. In the integration the spectra were weighted by the particle detection efficiency function, $f_p(\vartheta_p)$. As a result we have got a less sharp and more asymmetric cusp peak. We used this spectrum shape to fit the measured TDCS values [see the curves through the data in Fig. 3(b)]. A reasonable fit was obtained, although the cusp in the convoluted zero-degree spectrum is still less asymmetric than those observed at large-angle scatterings. At each of the observation angles most of the TDCS data at the high-energy tail of the peak lie below the curve of the ''model'' spectrum. The fall of the data is particularly steep for the angles 3.7° and 5.0°. The data at the low-energy tail of the peak follow the curve of the model spectrum quite well, except 8.1°, where an abrupt rise of the cross section towards small electron energies can be observed. The reason for the latter behavior is unknown.

In Fig. 4 the result of the other type of coincidence experiment carried out in the arrangement shown by Fig. 2(b) is presented. In this experiment the electrons emitted at 0° were detected in coincidence with the protons scattered at 6.8°. As was discussed in the Introduction, with this experiment our aim was to decide the question whether the incoming phase of the collision also contributes to the electron cusp, or the peak is completely formed in the outgoing part of the collision. For a comparison, in Fig. 4 we have also plotted the TDCS values for the case $\vartheta_e = \vartheta_p = 6.8°$. These latter data were obtained interpolating between the TDCS

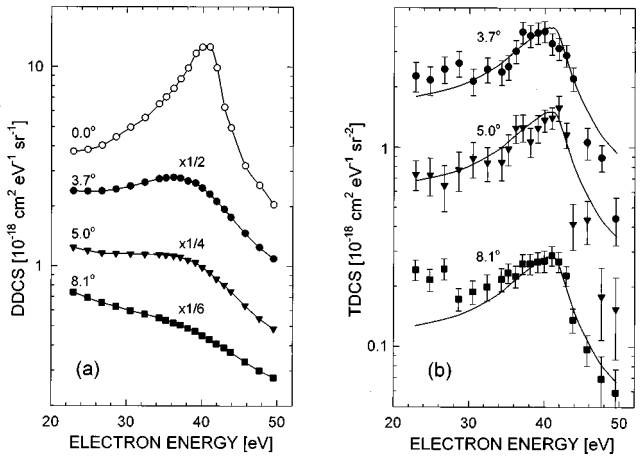


FIG. 3. Measured doubly (a) and triply (b) differential cross sections for electron emission in collisions of 75 keV protons with Ar atoms. TDCS's belong to $\vartheta_e = \vartheta_p$. Open circles, 0°; full circles, 3.7°; full triangles, 5.0°; full squares, 8.1°. The factors 1/2, 1/4, and 1/6 have been applied to the DDCS values for the sake of better visualization. The curves through the data in (a) are drawn only to guide the eye. The curves in (b) are results of fits using a function that was determined from separate noncoincidence measurements around 0° (see text).

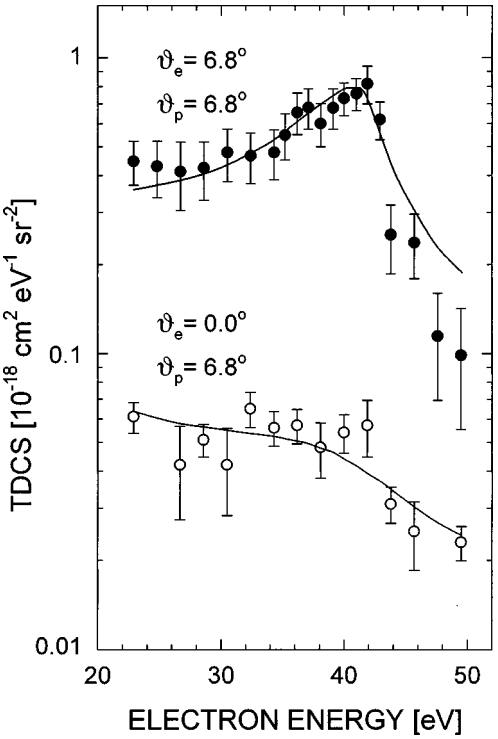


FIG. 4. Comparison of TDCS's obtained with different relative positions of the electron spectrometer and the particle detector. Full circles, $\vartheta_e=\vartheta_p=6.8°$; open circles, $\vartheta_e=0°$ and $\vartheta_p=6.8°$. The curves through the data are results of fits using functions that were determined from shapes of ''singles'' spectra taken around 0° (upper curve) and at 6.8° (lower curve).

values belonging to 5.0° and 8.1° [see Fig. 3(b)]. The cross sections for $\vartheta_e=0°$ and $\vartheta_p=6.8°$ are smaller than those for $\vartheta_e=\vartheta_p=6.8°$ by about one order of magnitude, and they do not show any peak structure. Similarly, as we did for the TDCS data in Fig. 3(b), we again compared the coincidence spectrum with that taken in a separate noncoincidence experiment. Now, considering that the relative observation angle between the electrons and the outgoing protons is 6.8°, the noncoincidence spectrum was taken at that angle. The obtained spectrum shape was found to be in reasonable agreement with that of the coincidence spectrum (see the curve through the TDCS data for the case $\vartheta_e=0°$ and $\vartheta_p=6.8°$ in Fig. 4). We note that further measurements are needed to reduce the statistical errors of the coincidence data and to rule out the presence of the peak completely. This is difficult, because the cross sections are very small and the number of the random coincidences is very large due to the high count rate in the electron branch at $\vartheta_e=0°$. In any case, we may conclude from the comparison of the two TDCS data sets in Fig. 4 that the overwhelming majority of the electrons ejected from the target with velocities around $v_e=v_p$ follow the scattered protons, and only a small part of those electrons fly in the forward direction. This strong directional correlation reflected by the TDCS data is surprising, because the DDCS data in Fig. 3(b) show a strong angular dependence only close to the cusp maximum, but at the ends of the energy interval of the measurement (22 and 50 eV) the variation of the cross section with the angle is within a factor of 2. [Note that in the latter figure—for the sake of

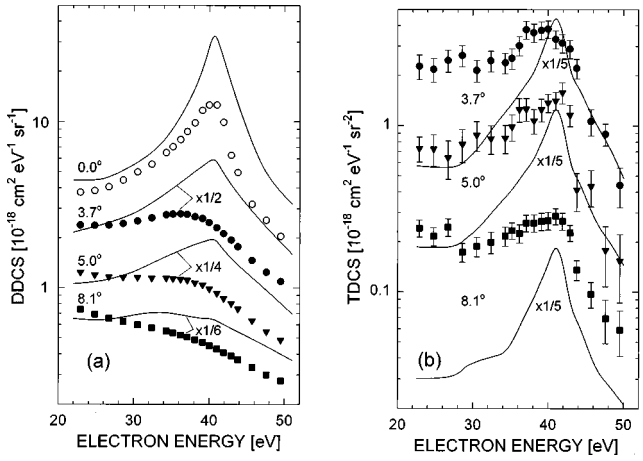


FIG. 5. Comparison of the measured DDCS and TDCS data with results of distorted-wave Born calculations. The notations of the experimental data are the same as in Fig. 3.

better visualization of the data—we applied factors 1/2, 1/4, and 1/6 to the DDCS values at angles $\vartheta_e=3.7°$, $\vartheta_e=5.0°$, and $\vartheta_e=8.1°$, respectively.] In contrast to this, in Fig. 4 the change of the TDCS values going from $\vartheta_e=6.8°$ to $\vartheta_e=0°$ is large also at the ends of the energy interval, it is a factor of about 5. Of course, one cannot compare the DDCS and TDCS data directly, because they belong to different regions of the impact parameter.

We compared the results of the experiments with calculations made in the first-order *distorted-wave Born* (DWB) approximation and in a *classical trajectory Monte Carlo* (CTMC) model. The comparison with the quantum mechanical description is shown in Fig. 5 and Fig. 6. For calculations

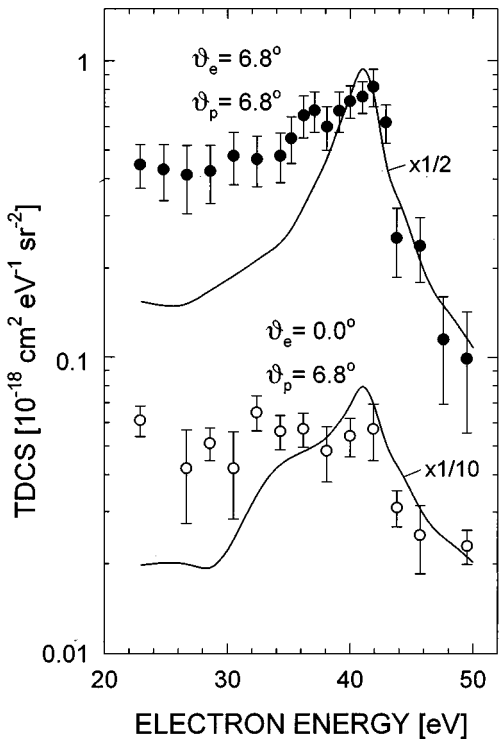


FIG. 6. Comparison of the TDCS data of Fig. 4 with results of distorted-wave Born calculations.

of DDCS's we used the CDW-EIS (continuum-distorted-wave–eikonal-initial-state) model [15], which is known to be a very efficient theory for the description of the continuous electron ejection in ion-atom collisions [3]. As is seen from Fig. 5(a), the results obtained by the CDW-EIS model are only in a qualitative agreement with the experimental DDCS data. The cusp predicted by the model is sharper and more symmetric than the observed one. The model considerably overestimates the cross section. Deviations of almost a factor of 3 occur at the cusp maximum at $\vartheta_e = 0°$. The agreement between theory and experiment becomes better with increasing observation angle. The reason for the discrepancy is that the collision velocity is too small for the applicability of a first-order description. The two-center character of the collision is not taken into account properly by the model, this explains why the cusp is overestimated and symmetric.

Concerning calculations of TDCS's, the following model was used. The dependence of the cross section on the scattering angle of the projectile can be expressed in the simplest way by the impact-parameter description of the ionization process [16]

$$\frac{d^3\sigma}{dE_e d\Omega_e d\Omega_p} = \left(\frac{d\sigma}{d\Omega_p}\right)^{\text{scatt}} \frac{d^2P(b)}{dE_e d\Omega_e}, \tag{4}$$

where $(d\sigma/d\Omega_p)^{\text{scatt}}$ is the cross section for the scattering of the projectile on the target atom, and $d^2P(b)/dE_e d\Omega_e$ is the ionization probability calculated along the classical trajectory of the projectile at impact parameter $b$. Unfortunately, before the present analysis there existed only such a version of the CDW-EIS model that assumed straight-line trajectory for the projectile path [17]. In the present work, describing the path of the projectile, we used the so-called ''broken-line'' approximation (see, e.g., [18]) in which the real projectile trajectory is replaced by its two asymptotes. This approximation is justified regarding the small proton scattering angles in the studied collisions. For calculation of $d^2P(b)/dE_e d\Omega_e$ the DWB approximation [3] was used in which the distortion of the electronic wave function is also expressed approximatively, by a multiplicative factor as suggested by Salin [19]. As is seen from Fig. 5(b), the simplified DWB calculations yielded similar sharp cusps at each observation angle as the cusp of the CDW model in Fig. 5(a). The calculated TDCS values are again much larger than the measured ones, and the theory is unable to reproduce the observed large asymmetry of the cusp.

Since the form of the ionization amplitude in the broken-line approximation is symmetric for the incoming and outgoing part of the projectile trajectory, one expects a cusp also at the conditions of our ''second-type'' experiment. This can be understood regarding that the distortion factor depends on the velocity vector of the projectile $\vec{v}_p(t)$, and it diverges at $\vec{v}_e = \vec{v}_p$. For the incoming part of the trajectory the direction of the projectile velocity coincides with that of the beam direction, therefore a cusp is expected to arise at 0°, regardless of the fact that projectile scatters into large-angle directions. Indeed, the calculations for $\vartheta_e = 0°$ and $\vartheta_p = 6.8°$ have resulted in TDCS values that show a cusp (see Fig. 6), although this cusp is broader than those obtained for the case $\vartheta_e = \vartheta_p$. This finding is in complete disagreement with the experiment. The shape of the calculated curve does not follow the tendency of the measured data, and the theoretical TDCS values are larger than the measured ones by a factor of about 10.

It is an interesting question whether the cusp due to precollision interaction is only an artifact of the approximations of the above theoretical model, or it would appear also in the exact quantum mechanical description of the ionization process. Lacking such a theory, one can say that a less pronounced precollision cusp would be obtained, if the broken-line trajectory were replaced by a more realistic one, e.g., hyperbolic trajectory. In this case the peak would be washed out to some extent by the continuous time dependence of $\vec{v}_p(t)$. [In the broken-line approximation the peak is enhanced due to the step-function-like behavior of $\vec{v}_p(t)$.] Furthermore, the first-order approximation corresponds to a picture of a *sudden* transition between the initial and final states that can take place with considerable probability in the incoming phase of the collision, leading to the precollision cusp. However, in a real collision the transition is not sudden, the wave function smoothly evolves in time. The electron ejected in the incoming phase at a given time moment will be influenced by the projectile at later time moments. Due to these secondary interactions, the electron will follow the projectile, even if the latter scatters into large angles (Coulomb focusing). Consequently, no strong precollision cusp is expected to occur in higher-order descriptions of the ionization process.

The CTMC simulations were made in the three-body approximation, i.e., the many-electron target atom was replaced by a one-electron atom. The core of the target ion was represented by a model potential developed by Green [20] based on Hartree-Fock calculations. It has the following form for a neutral atom:

$$V(r) = -[(Z-1)\Omega(r)+1]/r, \tag{5}$$

where $Z$ is the nuclear charge and

$$\Omega(r) = \{(\eta/\xi)[\exp(\xi r)-1]+1\}^{-1}.$$

Concerning the parameters $\eta$ and $\xi$, the values obtained by Garvey, Jackman, and Green [21] were used, $\eta = 3.50$ and $\xi = 0.957$ (in atomic units) for Ar.

The calculations were made in three dimensions as described by Olson and Salop [22] using the initialization parameters proposed by Reinhold and Falcón [23] for non-Coulombic interaction. The scattering of the projectile was described in a realistic way using the screened potential given by Eq. (5). In Fig. 7 we plotted the scattering angle as a function of the impact parameter. As is seen, in the angular range of the present study the scattering of the projectile is not a pure Rutherford scattering.

The initial position and momentum values of the target electron were randomly chosen in such a way that the binding energy was kept constant, 0.579 a.u. The Newton's equations of motion were solved by numerical integration using a Runge-Kutta method. The scheme of the calculation procedure was the same as it is given in the paper of Tökési and Mukoyama [24].

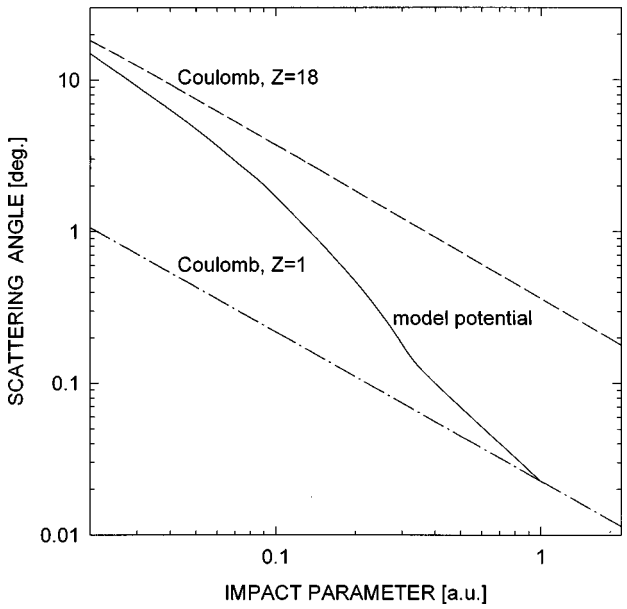


FIG. 7. Dependence of the scattering angle on the impact parameter. The dashed and dashed-dotted lines represent the Rutherford-scattering formula assuming nuclear and ionic charge, respectively. The full curve was obtained from the present classical trajectory Monte Carlo calculations using the model potential given by Eq. (5).

We made two separate computer runs for calculations of DDCS's and TDCS's. For DDCS's we regarded $4\times10^6$ collision events. The obtained cross sections are compared with the experimental data in Fig. 8(a). For a better comparison of the spectrum shapes, in the figure we multiplied the theoretical values by factor of 3. As is seen, the shape of the cusp, particularly the asymmetry of the peak, is better reproduced by the classical theory than by the quantum mechanical one. This is due to the fact that the two-center character of the collision is described exactly in the CTMC model, but it is treated very approximatively in the CDW-EIS model.

Concerning TDCS's, we made the calculations for two scattering angles, $\vartheta_p=3.7°$ and $\vartheta_p=8.1°$. Although in this case the impact parameter range was better defined (by the known scattering angles) than it was for calculation of DDCS's, to achieve sufficient statistical accuracy still we had to regard large number of collisions, $4\times10^6$ events at each scattering angle. The obtained TDCS values are compared with the experimental data in Fig. 8(b). For the case $\vartheta_e=\vartheta_p=3.7°$ the agreement with the data is excellent both in shape and absolute scale. For $\vartheta_e=\vartheta_p=8.1°$ the agreement is worse, the cusp predicted by the theory is more pronounced than the observed one. To check the existence of the ''precollision'' cusp, we did not make separate CTMC calculations at $\vartheta_p=6.8°$, therefore we could not compare our experimental data directly with the theory. However, for the sake of a qualitative analysis in Fig. 8(b) we also plotted the TDCS values belonging to $\vartheta_e=0°$ and $\vartheta_p=8.1°$. These latter data do not show any peak structure, i.e., in the classical description of the ionization—in accordance with the experiment—we can exclude the cusp formation via precollision interaction.

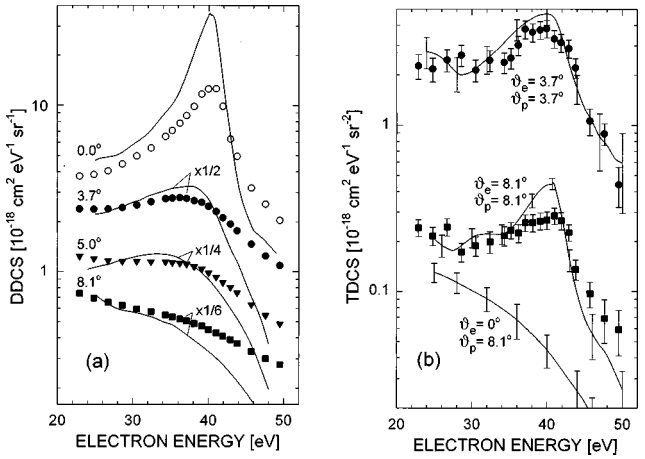


FIG. 8. Comparison of the measured DDCS and TDCS data with results of classical trajectory Monte Carlo calculations. The notations of the experimental data are the same as in Fig. 3. In (a) all of the theoretical values are multiplied by a factor of 3 (this factor is not shown in the figure).

## IV. CONCLUSIONS

In the present work we demonstrated the feasibility of measuring triply differential cross sections for the ECC cusp in ion-atom collisions. The cross sections are differential with respect to the energy and angle of the ejected electron ($E_e$ and $\vartheta_e$), as well as the angle of the scattered projectile ($\vartheta_p$). To verify experimentally that the ECC cusp is a result of final-state interaction between the electron and the outgoing projectile, we regarded the special case $\vartheta_e=\vartheta_p$ at nonzero-degree scattering angles. The appearance of the cusp in the energy spectrum confirms the picture based on the final-state interaction. As a further result of the work, we did not observe the cusp for electron emission at $\vartheta_e=0°$ accompanied by large-angle projectile scattering, i.e., we excluded the cusp formation via precollision interaction. A reasonable description of the experimental data was achieved by the classical trajectory Monte Carlo calculations. The agreement with the first-order quantum mechanical calculations is worse, and it is questionable whether the precollision cusp predicted by the latter theory will exist in the exact quantum mechanical description of the ECC process. It should be noted that the detection of the scattered projectiles was not completely optimized in the present experiment. With a more efficient particle detection one could increase the coincidence yield considerably, and the obtained data could be used for a more thorough comparison with the theories. As an example, we may mention that one could reduce the smearing of the cusp that arises from the finite angular resolution of the particle detector. This could be done by detecting the particles in a smaller solid angle.

## ACKNOWLEDGMENTS

This work was supported by the Hungarian Scientific Research Foundation (OTKA, Grant Nos. 3011, T022950, and F022059) and by the Deutsche Forschungsgemeinschaft (DFG).

[1] G. B. Crooks and M. E. Rudd, Phys. Rev. Lett. **25**, 1599 (1970).
[2] J. Berakdar, Phys. Rev. Lett. **78**, 2712 (1997); G. Gasane, F. D. Colavecchia, C. R. Garibotti, J. E. Miraglia, and P. Macri, Phys. Rev. A **55**, 2809 (1997).
[3] P. D. Fainstein, V. H. Ponce, and R. D. Rivarola, J. Phys. B **24**, 3091 (1991).
[4] J. E. Miraglia and J. Macek, Phys. Rev. A **43**, 5919 (1991).
[5] D. H. Jakubaßa-Amundsen, Nucl. Instrum. Methods Phys. Res. B **86**, 82 (1994).
[6] L. Sarkadi, J. Bossler, R. Hippler, and H. O. Lutz, Phys. Rev. Lett. **53**, 1551 (1984).
[7] A. Skutlarz, S. Haggmann, and H. Schmidt-Böcking, J. Phys. B **21**, 3609 (1988).
[8] O. Jagutzki, R. Koch, A. Skutlarz, C. Kelbch, and H. Schmidt-Böcking, J. Phys. B **24**, 993 (1991).
[9] A. Salin, J. Phys. B **2**, 631 (1969).
[10] J. Macek, Phys. Rev. A **1**, 235 (1970).
[11] L. Víkor, P. A. Závodszky, L. Sarkadi, J. A. Tanis, M. Kuzel, A. Báder, J. Pálinkás, E. Y. Kamber, D. Berényi, and K. O. Groeneveld, J. Phys. B **28**, 3915 (1995).
[12] G. Bernardi, P. Focke, and W. Meckbach, Phys. Rev. A **55**, R3983 (1997).
[13] M. E. Rudd, L. H. Toburen, and N. Stolterfoht, At. Data Nucl. Data Tables **23**, 405 (1979).
[14] T. Vajnai, A. D. Gaus, J. A. Brand, W. Htwe, D. H. Madison, R. E. Olson, J. L. Peacher, and M. Schulz, Phys. Rev. Lett. **74**, 3588 (1995).
[15] D. S. F. Crothers and J. F. McCann, J. Phys. B **16**, 3229 (1983).
[16] P. T. Greenland, J. Phys. B **14**, 3707 (1981).
[17] P. D. Fainstein, L. Gulyás, and A. Salin, J. Phys. B **29**, 1225 (1996).
[18] J. U. Andersen, L. Kocbach, E. Lægsagaard, M. Lund, and C. D. Moak, J. Phys. B **9**, 3247 (1976).
[19] A. Salin, J. Phys. B **5**, 979 (1972).
[20] A. E. S. Green, Adv. Quantum Chem. **7**, 221 (1973).
[21] R. H. Garvey, C. H. Jackman, and A. E. S. Green, Phys. Rev. A **12**, 1144 (1975).
[22] R. E. Olson and A. Salop, Phys. Rev. A **16**, 531 (1977).
[23] C. O. Reinhold and C. A. Falcón, Phys. Rev. A **33**, 3859 (1986).
[24] K. Tökési and T. Mukoyama, Bull. Inst. Chem. Res., Kyoto Univ. **72**, 62 (1994).